

## Supplementary Information

### Three-dimensional porous bowl-shaped carbon cages interspersed with carbon coated Ni-Sn alloy nanoparticles as high-performance lithium ion battery anode

Zhiyuan Wang,<sup>\*a,b,c</sup> Dan Wang,<sup>a,b,c</sup> Shaohua Luo,<sup>a,b,c</sup> Shuo Bao<sup>a</sup>, Yanguo Liu,<sup>a,b,c</sup> Xiwei Qi,<sup>a,b,c</sup> Chunlian He,<sup>d</sup> Chunsheng Shi,<sup>d</sup> Naiqin Zhao,<sup>d</sup>

<sup>a</sup> School of Materials Science and Engineering, Northeastern University, Shenyang 110819, P.R. China;

<sup>b</sup> School of Resources and Materials, Northeastern University at Qinhuangdao, Qinhuangdao 066004, P.R.China;

<sup>c</sup> Key Laboratory of Dielectric and Electrolyte Functional Material Hebei Province, Qinhuangdao, P.R. China;

<sup>d</sup> School of Materials Science and Engineering, Tianjin University, Tianjin 300072, P.R. China.

**\* Corresponding author**

**E-mail: zhiyuanwang@neuq.edu.cn;**

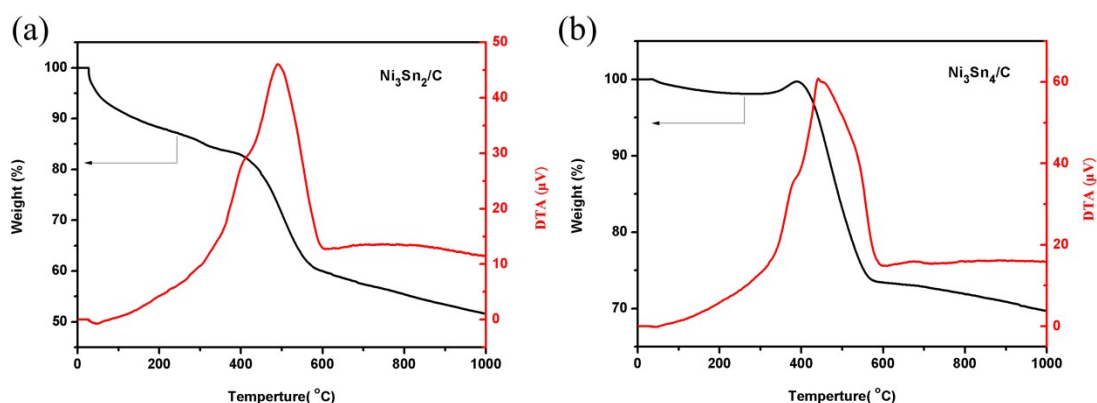


Fig. S1. TG-DTA curves of the  $\text{Ni}_3\text{Sn}_2/\text{C}$  and  $\text{Ni}_3\text{Sn}_4/\text{C}$  composite in air.

Thermogravimetric and differential thermal analysis (TG-DTA) was conducted in air to determine the contents of Ni-Sn alloy and carbon in  $\text{Ni}_3\text{Sn}_2/\text{C}$  and  $\text{Ni}_3\text{Sn}_4/\text{C}$  composite, as shown in Figure S1. The samples are annealed under air to oxidize Sn to  $\text{SnO}_2$ , Ni to NiO, and carbon to  $\text{CO}_2$ . On the basis of the final weight of NiO and  $\text{SnO}_2$ , the original content of  $\text{Ni}_3\text{Sn}_2$  and  $\text{Ni}_3\text{Sn}_4$  are calculated according to the following equations to be 47.2 wt.% and 57.7 wt.%, respectively, which are in accordance with the design values ( $\text{Ni}_3\text{Sn}_2:\text{C}=1:40$ , mass fraction of  $\text{Ni}_3\text{Sn}_2$  is 46.3

%;  $\text{Ni}_3\text{Sn}_4\text{:C}=1\text{:}40$ , mass fraction of  $\text{Ni}_3\text{Sn}_2$  is 57.5 %).

$$\text{Ni}_3\text{Sn}_2(\text{wt}\%) = \frac{\text{final weight of product} \times \frac{3}{5} \times \frac{M_{\text{Ni}}}{M_{\text{NiO}}} + \text{final weight of product} \times \frac{2}{5} \times \frac{M_{\text{Sn}}}{M_{\text{SnO}_2}}}{\text{initial weight of Ni}_3\text{Sn}_4/\text{C composite}} \times 100\% \quad (\text{S1-1})$$

$$\text{Ni}_3\text{Sn}_4(\text{wt}\%) = \frac{\text{final weight of product} \times \frac{3}{7} \times \frac{M_{\text{Ni}}}{M_{\text{NiO}}} + \text{final weight of product} \times \frac{4}{7} \times \frac{M_{\text{Sn}}}{M_{\text{SnO}_2}}}{\text{initial weight of Ni}_3\text{Sn}_4/\text{C composite}} \times 100\% \quad (\text{S1-2})$$

In order to verify whether there was residual NaCl in the products after washing, EDS examination (element mapping of Na and Cl) was conducted, as shown in Fig. S2. The NaCl template cannot be completely removed even after washing with water. There will be trace Na and Cl residual in the final products. However, the content of Na and Cl is very little, as shown in the EDS data (Fig.S2).

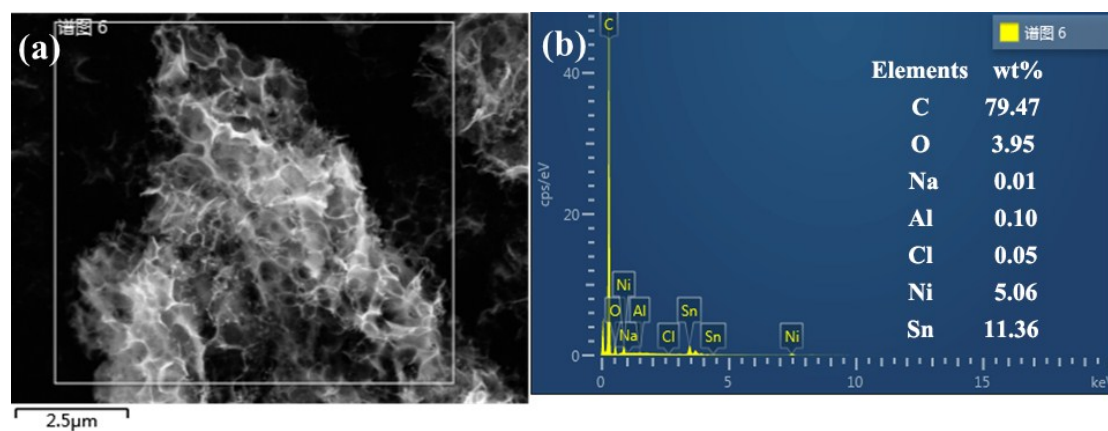


Fig. S2. The SEM and EDS element mapping data of  $\text{Ni}_3\text{Sn}_4/\text{C}$  sample after washing.

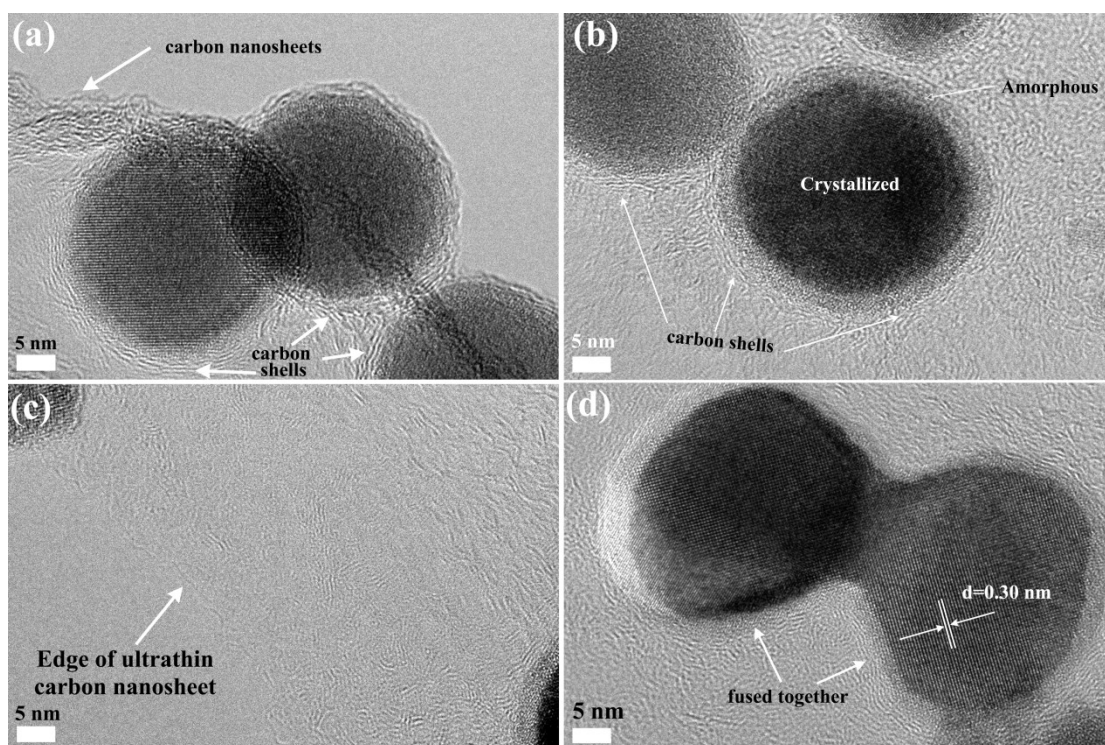


Fig. S3. HRTEM images of  $\text{Ni}_3\text{Sn}_4/\text{C}$  taken from different representative parts.

In order to demonstrate the effect of Ni in the unique nanostructure, we prepared reference sample of Sn embedded in 3D porous carbon cages and compared its electrochemical performance with that of the design samples. The reference sample is well-matched with Sn (PDF:65-0296), and the morphology of reference sample (Sn/C) is very similar with that of  $\text{Ni}_3\text{Sn}_4/\text{C}$  and  $\text{Ni}_3\text{Sn}_2/\text{C}$ . Fig.S4 (c) shows the CV plots of Sn embedded in the 3D porous carbon cages, which is very similar with the CV curves of Sn/C anode in the literatures<sup>[S1,S2]</sup>. What's more, the cycling capability of Sn/C,  $\text{Ni}_3\text{Sn}_4/\text{C}$ , and  $\text{Ni}_3\text{Sn}_2/\text{C}$  for 100 cycles are compared in Fig.S4(d). The capacity of Sn/C decreased rapidly with cycling, while the capacity of  $\text{Ni}_3\text{Sn}_4/\text{C}$  and  $\text{Ni}_3\text{Sn}_2/\text{C}$  gradually increased with cycling. When the cells after 100 cycles were disassembled, we found the active material Sn/C have fallen off the current collector, while the  $\text{Ni}_3\text{Sn}_4/\text{C}$  and  $\text{Ni}_3\text{Sn}_2/\text{C}$  were adhered firmly to the current collector. This indicates that the Ni in Ni-Sn alloy plays a role to restrain the volume change and enhance the stability of the composite anode.

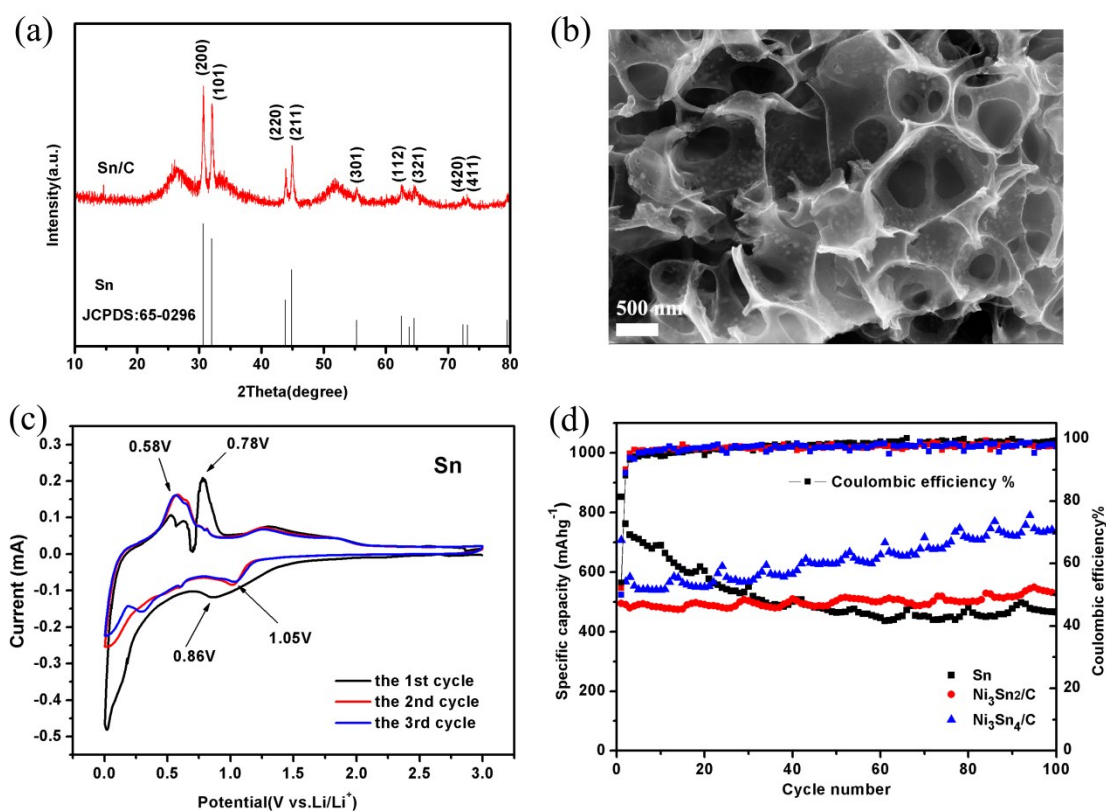


Fig.S4 The reference sample of Sn embedded in the 3D porous carbon cages prepared by the same method.

(a) XRD pattern of Sn/C; (b) SEM images of Sn/C; (c) CV plots of Sn/C; (d) Cycling performance of Sn/C,  $\text{Ni}_3\text{Sn}_4/\text{C}$ , and  $\text{Ni}_3\text{Sn}_2/\text{C}$  for 100 cycles.

The morphology of  $\text{Ni}_3\text{Sn}_4/\text{C}$  electrode after 200 cycles were explored by SEM and TEM, as shown Fig. S5. It can be clearly seen from Fig. S5 (a,b) (SEM) that the three-dimensional porous bowl-shaped carbon cages were well kept after repeated cycling. However, the  $\text{Ni}_3\text{Sn}_4$  nanoparticles cannot be observed because the surface was covered with SEI film. Fig. S5 (c,d) (TEM) displays that the monodisperse nanoparticles with diameter of 15~30 nm have not aggregated and still firmly embedded in the three-dimensional porous bowl-shaped carbon cages, which is very similar to the morphology of the original sample. The SEM and TEM results demonstrates the stability of the unique structure. In addition, this indicates that there is a strong interaction between carbon coated  $\text{Ni}_3\text{Sn}_4$  nanoparticles and the three-dimensional porous bowl-

shaped carbon cages, which is favorable for the cycling stability.

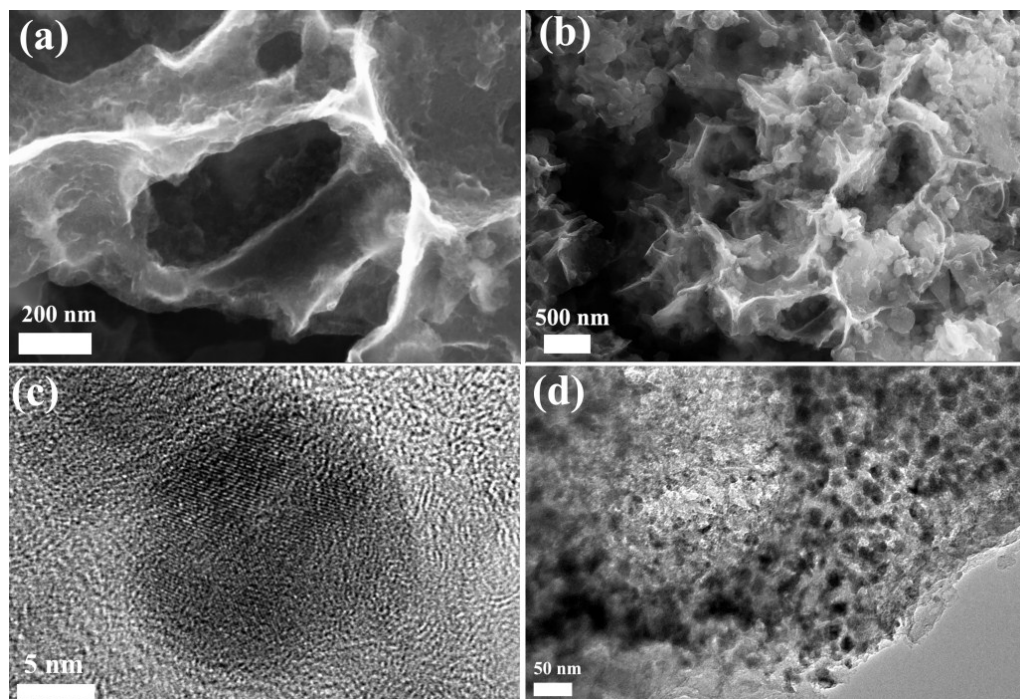


Fig. S5 SEM (a,b) and TEM (c,d) images of Ni<sub>3</sub>Sn<sub>4</sub>/C anode after 200 cycles.

To demonstrate the fast transmission of lithium ion in the unique Ni<sub>3</sub>Sn<sub>4</sub>/C nanostructure, cyclic voltammetry of cells made of Ni<sub>3</sub>Sn<sub>4</sub>/C under different scanning rate (0.2 mV s<sup>-1</sup>, 0.4 mV s<sup>-1</sup>, 0.6 mV s<sup>-1</sup>, 0.8 mV s<sup>-1</sup>, 1 mV s<sup>-1</sup>) were performed. The CV plots were shown in the following and supplementary information (Fig. S6), the diffusion coefficient of lithium ion was calculated via the CV plots according to Randles-Sevcik equation at room temperature.

$$\text{Randles-Sevcik equation: } I_p = 0.4463zFA(zF / RT)^{1/2} C_o D_{Li}^{1/2} \nu^{1/2}$$

$$\text{At room temperature: } I_p = 2.69 \times 10^5 n^{3/2} A D_{Li}^{1/2} \nu^{1/2} C_o$$

in which n is the number of electrons per reaction species (for Li<sup>+</sup> it is 1), A is the area of the electrode, the radius of electrode is 5 mm, so the area is 0.785 cm<sup>2</sup>; and C<sub>o</sub> is the bulk concentration of the Li<sup>+</sup> ion in the electrode (mol cm<sup>-3</sup>). D<sub>Li</sub> is the diffusion coefficient of Li in the electrode; At very slow scan rate, the peak current (i<sub>p</sub>) varies linearly with the scan rate (ν), as shown in Fig. S6(b), i<sub>p</sub> is proportional to ν<sup>1/2</sup>. From the slope of the linear fit, we have calculated

the diffusion coefficients  $D_{Li}$  corresponding to electrochemical lithiation reactions to be  $2.45 \times 10^{-7} \text{ cm}^2 \text{ s}^{-1}$ . The diffusion coefficient is higher than those in nano-sized Sn ( $8 \times 10^{-8} \text{ cm}^2/\text{s}$ ) and Sn/Cu<sub>6</sub>Sn<sub>5</sub> composite thin film electrode ( $1.91 \times 10^{-7} \text{ cm}^2/\text{s}$ ) [S3, S4]. Thus, the Ni<sub>3</sub>Sn<sub>4</sub>/C composite anode has better rate capability and cycle performance.

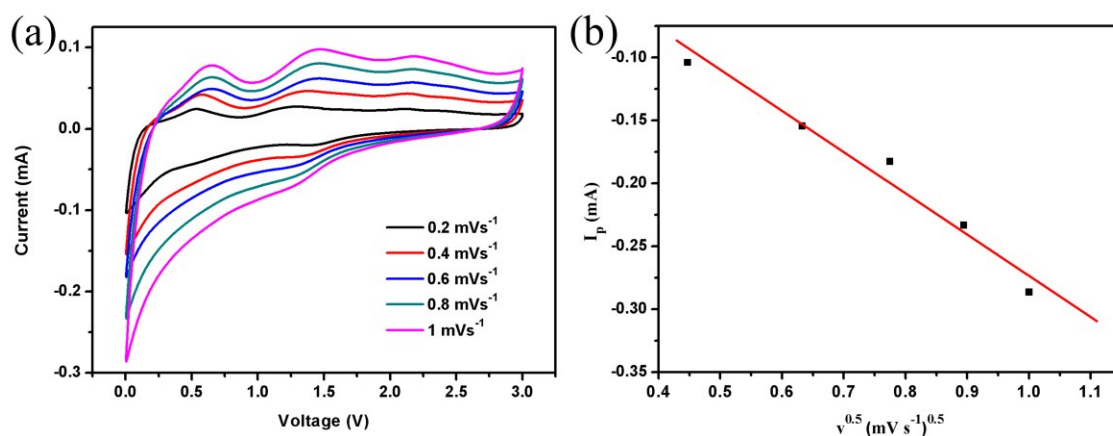


Fig. S6 (a) Cyclic voltammograms of Ni<sub>3</sub>Sn<sub>4</sub>/C for various scan rates; (b) peak current  $I_p$  as a function of square root of scan rate  $v^{1/2}$ .

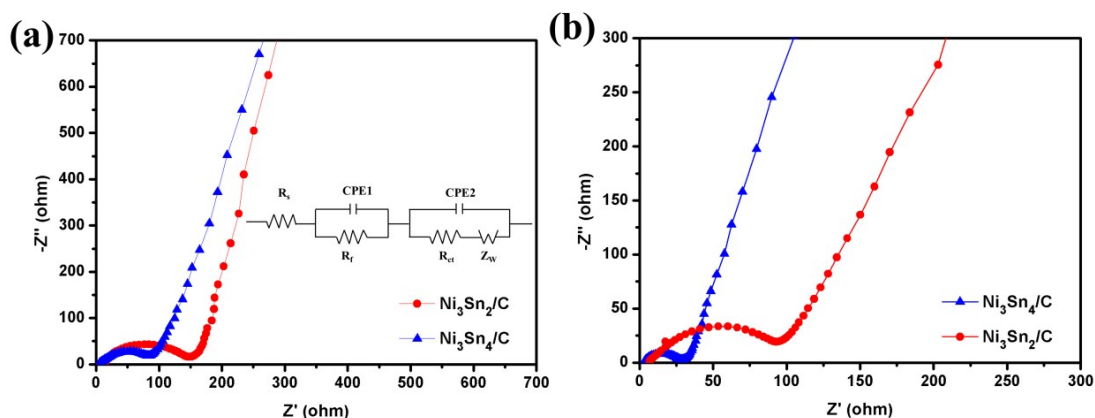


Fig. S7 (a) Nyquist plots of Ni<sub>3</sub>Sn<sub>2</sub>/C and Ni<sub>3</sub>Sn<sub>4</sub>/C electrodes before cycling and the corresponding equivalent circuit (embedded in); (b) Nyquist plots of Ni<sub>3</sub>Sn<sub>2</sub>/C and Ni<sub>3</sub>Sn<sub>4</sub>/C electrodes after 200 cycles.

$R_s$  is the electrolyte resistance,  $R_f$  is the resistance of the surface film (including SEI film impedance),  $R_{ct}$  is charge-transfer resistance,  $Z_w$  is the Warburg impedance related to the diffusion

of  $\text{Li}^+$  into the bulk electrodes and CPE represents the constant phase element.

Table S1 Kinetic parameters of the electrodes of  $\text{Ni}_3\text{Sn}_2/\text{C}$  and  $\text{Ni}_3\text{Sn}_4/\text{C}$  composite before cycling.

Samples		$R_f$ ( $\Omega$ )	$R_{ct}$ ( $\Omega$ )
$\text{Ni}_3\text{Sn}_2/\text{C}$	before cycling	32.8	116.8
	after 200 cycles	36.5	73.5
$\text{Ni}_3\text{Sn}_4/\text{C}$	before cycling	17.4	64.8
	after 200 cycles	26.2	38.8

Table. S2 Initial capacity, cycle performance and rate capability of  $\text{Ni}_3\text{Sn}_2/\text{C}$ ,  $\text{Ni}_3\text{Sn}_4/\text{C}$  and some representative Ni-Sn alloy anodes in literatures.

Materials	1 <sup>st</sup> charge capacity Capacity/rate (mAh g <sup>-1</sup> /A g <sup>-1</sup> )	Cyclic Properties Capacity/current density/cycles (mAh g <sup>-1</sup> /A g <sup>-1</sup> /cycles)	Rate capability Current density: Capacity (A g <sup>-1</sup> : mAh g <sup>-1</sup> )	Reference
$\text{Ni}_3\text{Sn}_4/\text{C}$	735/0.1	740 /0.5/100	1: 577 2: 496	This work
$\text{Ni}_3\text{Sn}_2$ @reduced graphene oxide	874/0.1	554/0.1/200	0.8: 422 1.6: 300	S5
Sn@ $\text{Ni}_3\text{Sn}_4/\text{C}$	564/0.2	410/0.2/800	1: 248 2: 220	S6
Ni-Sn Intermetallic Microcages	464/0.1	399/0.1/400	0.6: 311 1.3: 267	S7
2D $\text{Ni}_3\text{Sn}_2$ @C@PGC)	531/0.114	585/0.114/100	1.14: 314 2.28: 188	S8
3D Ni-Sn nanowire networks	580/0.05	450/0.1/50	0.45: 450 2.2: 380	S9
3D porous Ni-Sn alloy	800/0.025	501/ 0.05/50	—	S10
Ni-Sn Nanostructured Electrodes	500/0.4	500/0.4 /200	0.75: 300 2: 200	S11

## Reference

(S1) Y. H. Xu, Q. Liu, Y. J. Zhu, Y. H. Liu, A. Langrock, M. R. Zachariah and C. S. Wang, *Nano Lett.*, 2013, **13**,

470-474.

- (S2) Z. Zhu, S. Wang, J. Du, Q. Jin, T. Zhang, F. Cheng and J. Chen, *Nano Lett.*, 2014, **14**, 153-157.
- (S3) T. Zhang, L.J. Fu, J. Gao, Y.P. Wu, R. Holze and H.Q. Wu, *J. Power Sources*, 2007, **174**, 770-773.
- (S4) R.Z. Hu, M.Q. Zeng and M. Zhu, *Electrochim. Acta*, 2009, **54**, 2843-2850.
- (S5) Z. Yi, X. Tian, Q. G. Han, Y. Cheng, J. S. Lian, Y. M. Wu and L. M. Wang, *Electrochim. Acta*, 2016, **192**, 188-195.
- (S6) X. Y. Hou, Y. J. H, H. Jiang, Y. F. Li, X. F. Niu and C. Z. Li, *Chem. Commun.*, 2015, **51**, 16373-16376.
- (S7) J. Liu, Y. R. Wen, P. A. V. Aken, J. Maier and Y. Yu, *Nano Lett.*, 2014, **14**, 6387-6392.
- (S8) J. Qin, X. Zhang, N. Q. Zhao, C. S. Shi, E. Z. Liu, J. J. Li and C. N. He, *RSC Adv.*, 2014, **4**, 49247-49256.
- (S9) M. Tian, W. Wang, S. H. Lee, Y. C. Lee and R. G. Yang, *J. Power Sources*, 2011, **196**, 10207-10212.
- (S10) L. Huang, H. B. Wei, F. S. Ke, X. Y. Fan, J. T. Li and S. G. Sun, *Electrochim. Acta*, 2009, **54**, 2693-2698.
- (S11) J. Hassoun, S. Panero, P. Simon, P. L. Taberna and B. Scrosati, *Adv. Mater.*, 2007, **19**, 1632-1635.